Robust design of compact microwave absorbers and waveguide matched loads based on DC-conductive 3D-printable filament

D. Meisak[1,2], E. Gurnevich[2], A. Plyushch[1,2]
D. Bychanok[1,3,*], V. Georgiev[4], R. Kotsilkova[5], P. Kuzhir[6,1]

[1] Institute for Nuclear Problems Belarusian State University, Bobruiskaya str. 11, Minsk, 220006, Belarus
[2] Faculty of Physics, Vilnius University, Sauletekio 9, LT-10222 Vilnius, Lithuania
[3] Tomsk State University, 36 Lenin Prospekt, Tomsk 634050, Russian Federation
[4] NanoTechLab Ltd. Acad. G. Bonchev str. 4, Sofia, 1113, Bulgaria
[5] OLEM, Institute of Mechanics Bulgarian Academy of Sciences, Acad. G. Bonchev str. 4, Sofia, 1113, Bulgaria
[6] Institute of Photonics, University of Eastern Finland, Yliopistokatu 7, FI-80101 Joensuu, Finland

E-mail: dzmitrybychanok@yandex.by

February 2020

Abstract. The design concept of effective microwave absorbers and compact matched loads based on 3D-printable lossy nanocarbon-based composites with filler content above the percolation threshold is proposed. The DC-conductive (σ_{DC}=0.39 S/m) 3D-printable filament based on poly(lactic) acid (PLA) filled with 12wt.% of multiwalled carbon nanotubes (MWCNTs) was used. The electromagnetic properties of 3D-printed pyramidal regular structures were experimentally investigated and numerically simulated in 12-18 GHz (Ku-band) and 26-37 GHz (Ka-band) frequency ranges. Within the proposed model the structures under study were considered as graded refractive index material. The optimal geometrical parameters of designed microwave components were successfully evaluated using numerical modeling. Tested components demonstrate remarkable shielding efficiency (> 20 dB) within whole Ku- and Ka-bands and are suitable for practical application related to effective absorption of microwave radiation. The production of 3D-printable materials with controlled and predicted losses offers the possibility for miniaturization of 3D printed microwave components, such as absorbers and loads. The developed technique, estimating the geometrical parameters of the components vs dielectric properties of the conductive filament, could be used as a versatile platform for predesign of compact microwave devices taking into account constituent dielectric parameters of available printable materials and filaments.

Keywords: 3D-printing, conductive 3D-printable filament, microwave electromagnetic response, Ku-band, Ka-band. Submitted to: *J. Phys. D: Appl. Phys.*

1. Introduction

The additive manufacturing offers the cheap and time saving possibility to produce devices and structures of complex shape and opens challenging opportunities for the design and engineering of microwave devices. The development of effective absorbers of electromagnetic radiation is very important for many actual practical problems related to electromagnetic compatibility [1–3]. The waveguide matched load is a common example of a device, which absorbs electromagnetic energy almost without reflecting the incident electromagnetic wave. Usually, the design of such components is based on a long wedge or pyramid placed in the center of the waveguide [4]. The wedge is made of lossy material (e.g., dispersed carbonyl iron particles in the epoxy resin) and its top is oriented to the incident wave source. The existence of the optimal value of complex dielectric permittivity (or electrical conductivity in the range of "several Siemens per meter" for microwave frequencies) for effective absorption in the material was shown previously [5, 6]. Nevertheless, in practice, it is often difficult to achieve optimal dielectric permittivity and control simultaneously both material losses and its mechanical properties. The losses in available conventional materials are often below optimal values leading to an increase in the length of the wedge to achieve the necessary level of electromagnetic attenuation.

The fabrication of 3D-printable components and materials with controlled and predicted losses offers the possibility for miniaturization of absorbers and loads. We will show that DC-conductive filament of intermediate electrical conductivity (i.e. $\simeq 1$ S/m) is a universal mean for microwave attenuation elements design by 3D printing. We will present the laboratory process for conductive filament production and then use it for 3D-printing of pyramidal structures to prove the proposed concept of light and compact matched loads.

The periodic pyramidal structures are used as broadband absorbers for the anechoic chambers [7, 8]. Viskadourakis *et al.* investigated the shielding efficiency of the lossless pyramidal structure in 3.5–7 GHz [1], Nornikman *et al.* studied the hexagonal pyramids [9] in 1-20 GHz, Jenks [10] applied the pyramidal structures as antenna for 3.3-8.0 GHz frequencies. However, all the mentioned components were produced from non-conductive plastics. The development of the lossy filament opens new possibilities for the 3D printing techniques in the field of electromagnetic interference (EMI) shielding applications [3].

The aim of the present paper is to study the possible application of 3D printing technology for the shielding components and matched loads design. The method of the optimal geometrical parameters evaluation is presented. The effectiveness of the method is verified by experimental studying the shielding performances of the printed structure.

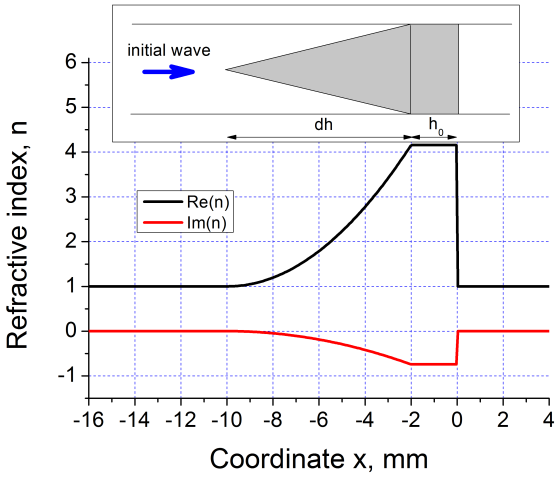

Figure 1. Spatial distribution of refractive index in the pyramidal structure after homogenization (inset: the side view of the pyramid inside the waveguide).

2. Model for electromagnetic properties simulation

The classical matched load working principle is based on a smooth transition from an empty waveguide to a waveguide filled with lossy material. The smooth transition is necessary to vanish the reflected power from inhomogeneity inside the waveguide. Usually, the lossy region is made in the shape of a long wedge or pyramid and placed in the center of the waveguide, which top oriented to the incident electromagnetic wave (Fig. 1 (inset)). The coordinate of the base of pyramid is assigned as ($x = 0$), dh is the pyramid's height, h_0 is the substrate (base of the pyramid) thickness. By propagation through the waveguide from the top of the pyramid to the base, the relative volume fraction of the lossy material increases and vice-versa the air fraction decreases. Since the transition is smooth, homogenization can be done and the pyramid may be considered as a structure with spatially distributed refractive index [11, 12]. In refs. [13,14] we showed experimentally and numerically that the scattering parameters of the homogenized layer are equivalent to the initial structure for spheres, hollow spheres, corrugated composites and similar structures inside the waveguide.

The cross-section of a waveguide along the plane perpendicular to the pyramid base consists of the rectangle-like lossy region and air region. The homogenization procedure, in this case, means that the air regions can be averaged with lossy regions according to their relative surface fractions $S(x)$. The

dependence of the effective refractive index n on the coordinate x is as follows [11, 14]:

$$n(x) = n_p(1 - S(x)) + n_0 S(x), \quad (1)$$

where

$$S(x) = \begin{cases} 1, x < -(h_0 + dh) \\ 1 - (\frac{h_0+dh+x}{dh})^2, -(h_0 + dh) < x < -h_0 \\ 0, -h_0 < x < 0 \\ 1, x > 0 \end{cases} \quad (2)$$

and $n_p = \sqrt{\varepsilon}$ is the refractive index of pyramid's bulk material, $n_0 = 1$ is the refractive index of air. The spatial distribution of refractive index $n(x)$ Eq.(1) is parabolic and presented in Fig. 1.

The relative amplitudes of reflected S_{11} and transmitted S_{21} trough the pyramid signals may be easily calculated using a multi-layered approach developed in optics and discussed in detail in [13–15]. The shielding efficiency SE is defined [16, 17] as $SE_T = -20 \log_{10} S_{21}$. Similarly, the efficiency due to reflectance is $SE_R = -20 \log_{10} S_{11}$.

The presented model gives the dependence of the shielding efficiency of pyramids placed in the waveguide transmission line on their geometrical parameters (h_0, dh) and dielectric properties (ε). Important to note, that in case of an array of pyramids inside the waveguide or in the free space it is enough to consider and perform averaging and homogenization within one unit cell. The model was implemented using MatLab software.

3. Samples preparation and characterization

3.1. Conductive filament production

The DC-conductive Graphene3D filament is based on the poly(lactic) acid (PLA) Ingeo^{TM} Biopolymer PLA-3D850 (Nature Works) with a 12wt.%-content of -OH modified multiwalled carbon nanotubes (MWCNTs) supplied by TimesNano, China. The following procedure was used to prepare DC-conductive Graphene3D filament ready for further 3D-printing.

Firstly, the masterbatch of 12 wt % MWCNTs was prepared by melt mixing of the filler and the polymer in the twin-screw extruder (COLLIN Teach-Line ZK25T) by setting a screw speed of 40 rpm and keeping the temperature in the range 170–180C. After that, the composite pellets were extruded by a single screw extruder (Friend Machinery Co., Zhangjiagang, China) in the temperature range 170–180 C and a screw speed of 10 rpm for producing filament for 3D printing (FDM) with 1.75 mm in diameter. Below we will call the obtained material as Graphene3D filament.

3.2. Filament properties and printing

Scanning electron microscopy (SEM) analysis was performed to get information about the dispersion of nanofiller in the PLA host and its effect on the microstructure. Fig.2(a,b) showed the surfaces of both neat PLA and 12 wt% MWCNT/PLA, respectively, after liquid nitrogen breakage of the filament. Very different fracture surfaces are visible for the tested PLA and composite filaments, which are largely attributed to their brittle or ductile mechanical behavior. The neat PLA surfaces appear very flat due to the ductile fracture type, typical for an isotropic polymeric material. In contrast, a network type structure is developed over the entire surface of the MWCNT/PLA composite, due to the interconnection of well-dispersed MWCNTs and to a fine structure of micro-voids that is typical for a more brittle material.

In general, the network filler–polymer microstructure, formed by the strong and conductive MWCNTs in the PLA matrix is typically associated with percolation, which may result in enhanced mechanical and physical properties of nanocomposites compared to the neat PLA. The details of mechanical properties, electrical and thermal conductivity and electromagnetic shielding efficiency of both neat PLA and 12 wt% MWCNT/PLA filaments, obtained from our previous studies [3, 18, 19] are summarized in Table 1. As seen, the addition of 12 wt% MWCNTs enhance significantly mechanical properties of the filament, e.g. tensile elastic modulus and hardness, but decrease twice the elongation at ultimate strength, compared to the neat PLA. Moreover, the composite filament demonstrates twice higher thermal conductivity, compared to the PLA. This confirms the microstructural prediction, that the percolation structure of 12 wt% MWCNTs in the nanocomposite filament is highly conductive, lossy and stronger, but more brittle, than the neat PLA.

The improvement of Young's modulus (21%), hardness (11%) and electrical conductivity (10 decades) could be associated with the dense, conductive network structure formed by the carbon nanotubes above the percolation threshold, which allows a transfer of the extraordinary mechanical and electrical properties of carbon nanotubes through the polymer. In contrast, a twice decrease of % elongation of the composite filament compared to the neat PLA may be attributed to the large surface area of the filler which absorbs most of the polymer at the interfaces, as shown in Fig.2(b), which leads to increase of the brittleness of the composite material [3, 19]. However, the thermal conductivity of 12 wt% MWCNT/PLA filament was observed only twice higher compared to the neat PLA, in spite of the extremely high thermal conductivity of carbon nanotubes (3000 W/mK). This can be explained by the complex process of thermal diffusion

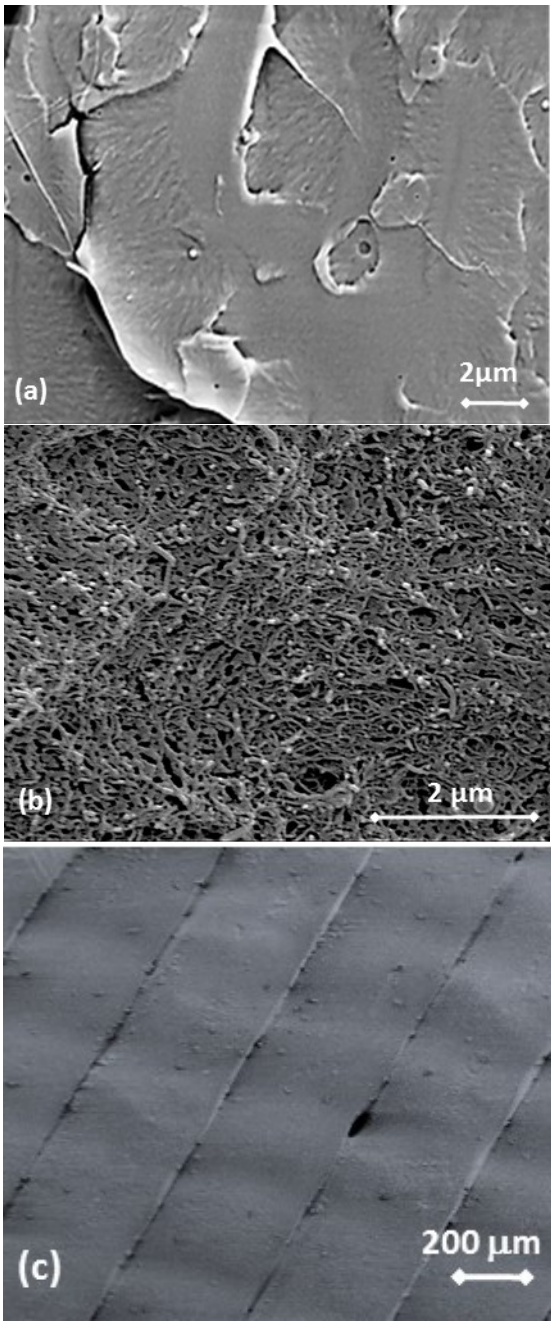

Figure 2. SEM images: the cross section of the PLA (a) and 12 wt.% MWCNT/PLA (b) filaments; (c) the surface of the 3D printed structure using 12 wt% MWCNT/PLA filament.

through a polymer, influenced by temperature, crystallinity, macromolecular orientation, etc. Moreover, carbon nanotubes within polymers are usually considered to have many defects that contribute to numerous phonon scatting lowering the thermal conductivity [18].

The fused deposition modeling (FDM-FFF)-type 3D printer X400 PRO German RepRap with an extrusion nozzle with a diameter of 0.5 mm was used. During printing, the filament was heated above its melting temperature and then extruded using a PC-controlled moving nozzle [3]. Thus, the desired 3D-structure is formed as a result of a layered process. The processing parameters of the 3D printing were a temperature of 200C, an extrusion speed of 100 mm/min, and the platform temperature of 60C. Samples were printed with 100% infill, in a rectangular direction of one layer to another, as shown in Fig.2(c).

3.3. Waveguide measurements

The microwave electromagnetic measurements performed using the waveguide method [20, 21]. A vector analyzer MICRAN R4M-18 with 16×8 mm^2 ~~(Fig. a)~~ and a scalar network analyzer Elmika R2-408R with 7.2×3.4mm^2 ~~(Fig. b)~~ waveguide systems were used for Ku- and Ka-bands, respectively. **Real images of waveguide systems are shown in the Fig.6** For both setups, the frequency dependencies of the scattering parameters, transmitted/input (S_{21}) and reflected/input (S_{11}) signals were measured.

4. Results

The complex dielectric permittivity and refractive index of the Graphene3D filament recalculated from experimentally measured S-parameters of the printed plane-parallel layer [20, 21] are presented in Fig. 3. The filament has high loss tangent (not less than 0.4 within the whole frequency range). Moreover, the material is dispersive, its dielectric permittivity is generally decreasing with frequency. This type of dispersion is typical for nanocarbon composites with filler content above the percolation threshold in microwave frequency range [22, 23].

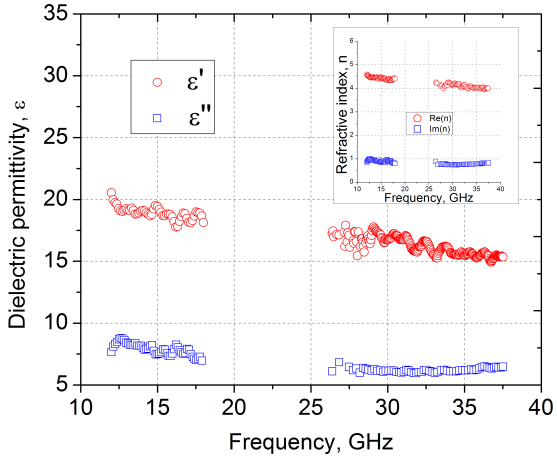

Figure 3. Frequency dependencies of dielectric permittivity and refractive index (inset) of the printed Graphene3D material in Ku- and Ka-bands.

Table 1. Mechanical and physical properties of the filaments.

Filament Type	Tensile Strength [MPa]	Tensile Young's Modulus [MPa]	Elongation [%]	Hardness [MPa]	Electrical Conductivity [S/m]	Thermal Conductivity [W/mK]
PLA	28.1±3.9	593.6±8.5	8.5±1.6	176±5	$8.3{\cdot}10^{-11}$	0.18±0.03
12wt.% MWCNT	23.3±1.9	719.9±6.2	4.3±0.4	195±9	0.39	0.37±0.02

The minimal height of pyramids and the substrate thickness were computed using using proposed model Eq.(1)-(2). Several simplifications were made. The frequency was fixed as 30 GHz, the effective shielding criteria were introduced as $SE_T > 20$ dB and $SE_R > 20$ (this is equivalent to the absorption of more than 99% of the power of incident wave).

For the computations of dh, substrate height was taken as $h_0 = 2$ mm. In this case, SE of the pyramid is dependent only on its height and dielectric permittivity of used material. The combinations of dh and ε that satisfy the mentioned criteria for SE are presented as the regions in $\varepsilon''(\varepsilon')$ coordinates in Fig. 4. The decrease of the dh result in narrowing the region of possible ε combinations. The measured dielectric permittivity of the Graphene3D filament at 30 GHz is $\varepsilon = 16.74 - i6.17$ (Fig. 3). The minimal pyramid's height dh, required for the effective shielding is 8-9 mm for the Ka-band. Similarly, $dh = 22$ mm was evaluated for the Ku-band.

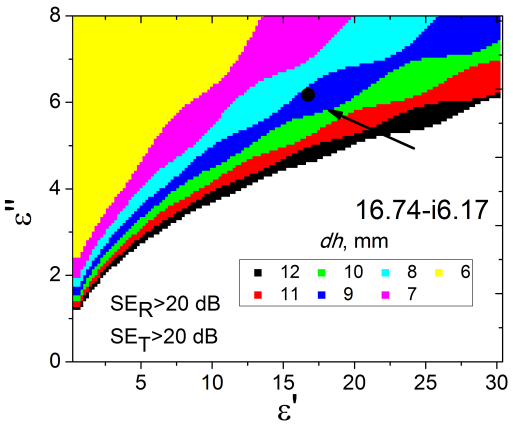

Figure 4. The pyramid height dh, required for the effective (20 dB) EMI shielding, presented as the dependence on the dielectric permittivity. Dot stands for the measured ε of Graphene3D filament at frequency 30 GHz.

For substrate thickness h_0 computations the obtained $dh = 8$ mm was used. The dependencies SE_T and SE_R on the substrate thickness h_0 are presented in Fig. 5 (filled symbols). The oscillations of SE_R related to the interference, while SE_T increases monotonously. These oscillations may be significantly dumped by increasing the height of the pyramids dh. The SE *vs* h_0 for the plane-parallel layer ($dh = 0$ mm) are also presented in Fig. 5 (see open symbols). Both SE_R and SE_T of the plane layer are significantly lower in comparison with the pyramidal structure. The SE_T expectedly increases with the thickness, but the SE_R remains lower than 5 dB. It means that a planar layer cannot simultaneously demonstrate high SE_R and SE_T parameters (or in other words absorption ability) at any substrate thickness.

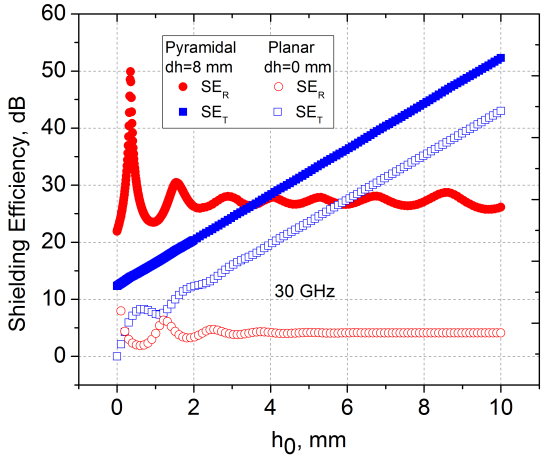

Figure 5. The dependence of the SE_T and SE_R on the substrate thickness. Pyramid heights are $dh = 8mm$ (close symbols) and $dh = 0mm$ (open symbols).

The proposed graded index approach is useful for the practical design of pyramidal matched loads. It provides the minimal geometrical parameters required for the effective SE taking into account the dielectric properties of used material. In particular case of the filament's permittivity, the combinations of $h_0 = 2$ mm, $dh = 8 - 9$ mm (Ka-band) and $dh = 22$ mm (Ku-band) are the minimal parameters, which allow to meet 20 dB level for both SE_T and SE_R.

The printed samples and the experimentally measured in Ku- and Ka-bands shielding efficiency are presented in Figs. 6 and 7, correspondingly.

Both structures for Ku- and Ka-bands demonstrate a high level of $SE_T > 20$ dB and $SE_R > 20$ dB, **even despite some printing issues (see Fig.6),** and may be used as effective matched loads or ab-

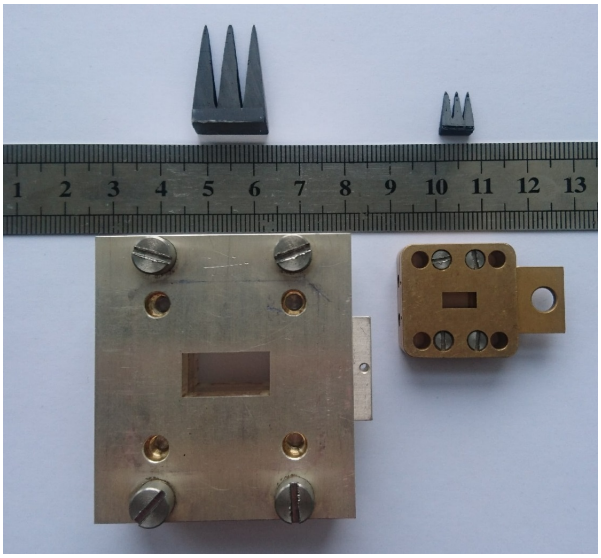

Figure 6. 3D printed pyramidal structures **and their corresponding waveguide systems** for Ku-band on the left and for Ka-band on the right.

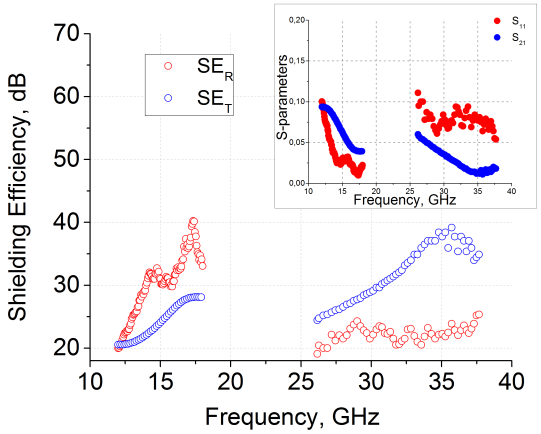

Figure 7. Shielding efficiency and S-parameters (inset) of the 3D printed samples in Ku- and Ka-bands.

sorbers in anechoic chambers. Usage of lossy material with high ε' and ε'' allows to obtain similar shielding performance with smaller pyramids (see Table 2). Even more, in contrast to the results listed in Table 2 [9, 24–28], we demonstrate that both transmitted and reflected signals are well attenuated. It is possible due to the combination of high Ohmic losses within the material bulk and waves scattering due to the sample's geometry. Important to note, that high Ohmic losses in considered materials were achieved because of forming DC conductive MWCNT-based network within the polymer matrix. Due to depolarization effects [23] the MWCNT agglomerates in the composite below percolation weakly interact with microwave radiation. Nevertheless, when agglomerates are incorporated in the percolative network of DC-conductive composite (which is exactly corresponds to our experimental situation) they contribute to effective scattering and attenuation of the electromagnetic waves.

5. Conclusions

The DC-conductive filament of 12 wt% MWCNT/PLA, suitable for 3D-printing was developed for effective absorbers and compact matched loads design. The pyramidal structures were 3D printed and experimentally tested in Ku- and Ka-bands. The pyramid height and the substrate thickness were obtained through the optimization of the shielding efficiency versus the complex permittivity of the filament. Measured shielding efficiency of the printed samples is higher than 20 dB both for reflected and transmitted signals in the investigated frequency ranges.

To conclude, the lossy periodic pyramidal structures 3D-printed from conductive filament are perspective for fabrication effective absorbers and waveguide matched loads. The developed technique for the pyramid parameters evaluation may be effectively used as a pre-experimental step since it takes into account the material properties (both for lossy and lossless), required frequency range, and the substrate thickness. This opens the road toward robust pre-design of compact microwave components taking into account constituent dielectric parameters of available printable materials and filaments.

Acknowledgments

The work is supported by H2020 RISE 734164 Graphene 3D. P.K. acknowledges the financial support from H2020-MSCA-IF-2018 project 836816 TURANDOT and Academy of Finland Flagship Programme, Photonics Research and Innovation (PREIN), decision 320166. D.B. is thankful for support by Tomsk State University Competitiveness Improvement Program. This research was also partially supported by the Belarusian Republican Foundation for Fundamental Research(BRFFR) project F18AZ-015. R.K. acknowledges the support from H2020-SGA-FET-Graphene Flagship-Graphene Core 3.

References

[1] Z Viskadourakis, KC Vasilopoulos, EN Economou, Costas M Soukoulis, and G Kenanakis. Electromagnetic shielding effectiveness of 3d printed polymer composites. *Applied Physics A*, 123(12):736, 2017.

[2] M Mirzaee, S Noghanian, and I Chang. Low-profile bowtie antenna with 3 d printed substrate. *Microwave and Optical Technology Letters*, 59(3):706–710, 2017.

Table 2. Comparison of the shielding performances of the pyramidal structures.

Material parameters	dh, mm	h_0, mm	SE_R, dB	SE_T, dB	Frequency, GHz	Reference
$\varepsilon = 2$, tanδ=0.2	90	25	45	n/a	10	[24]
$\varepsilon = 2.492$, tanδ=0.956	130	20	42.93	n/a	10-15	[9] *hexagonal
$\varepsilon = 2.9$, tanδ=0.084	130	n/a	43.294	n/a	10-15	[25] *triangonal
BlackMagic 3D	2	2	12	n/a	5.5	[26]
VeroBlack	80	20	20	n/a	100	[27]
$\varepsilon = 1.5$, tanδ=0.26	40	20	40	n/a	30	[28]
$\varepsilon = 18.66$, tanδ=0.38	22	2	40.15	28.09	17.4	this research
$\varepsilon = 15.55$, tanδ=0.39	8	2	23.88	39.17	35.7	this research

[3] Giovanni Spinelli, Patrizia Lamberti, Vincenzo Tucci, Rumiana Kotsilkova, Evgeni Ivanov, Dzhihan Menseidov, Carlo Naddeo, Vittorio Romano, Liberata Guadagno, Renata Adami, Darya Meisak, Dzmitry Bychanok, and Polina Kuzhir. Nanocarbon/poly(lactic) acid for 3d printing: Effect of fillers content on electromagnetic and thermal properties. *Materials*, 12(15):2369, 2019.

[4] David M. Pozar. *Microwave engineering*. John Wiley & Sons, 2009.

[5] Kevin Gaylor. Radar absorbing materials-mechanisms and materials. Technical report, 1989.

[6] Dzmitry Bychanok, Gleb Gorokhov, Darya Meisak, Polina Kuzhir, Sergey A Maksimenko, Yongliang Wang, Zhidong Han, Xin Gao, and Hongyan Yue. Design of carbon nanotube-based broadband radar absorber for ka-band frequency range. *Progress In Electromagnetics Research*, 53:9–16, 2017.

[7] B-K Chung H-T Chuah. Modeling of rf absorber for application in the design of anechoic chamber. *Progress In Electromagnetics Research*, 43:273–285, 2003.

[8] GE Hindman and Allen C Newell. Reflection suppression to improve anechoic chamber performance. *AMTA Europe*, pages 297–302, 2006.

[9] H Nornikman, F Malek, PJ Soh, and AA H Azremi. Reflection loss performance of hexagonal base pyramid microwave absorber using different agricultural waste material. In *2010 Loughborough Antennas & Propagation Conference*, pages 313–316. IEEE, 2010.

[10] CHJ Jenks. Dielectric pyramid antenna for gpr applications. In *2016 10th European Conference on Antennas and Propagation (EuCAP)*, pages 1–3. IEEE, 2016.

[11] D.G Stavenga, S Foletti, G Palasantzas, and K Arikawa. Light on the moth-eye corneal nipple array of butterflies. *Proceedings of the Royal Society of London B: Biological Sciences*, 273(1587):661–667, March 2006.

[12] Chih-Hung Sun, Peng Jiang, and Bin Jiang. Broadband moth-eye antireflection coatings on silicon. *Applied Physics Letters*, 92(6):–, 2008.

[13] DS Bychanok, AO Plyushch, GV Gorokhov, US Bychanok, PP Kuzhir, and SA Maksimenko. Microwave radiation absorbers based on corrugated composites with carbon fibers. *Technical Physics*, 61(12):1880–1884, 2016.

[14] D Bychanok, Sijin Li, A Sanchez-Sanchez, G Gorokhov, P Kuzhir, FY Ogrin, Andreea Pasc, T Ballweg, K Mandel, A Szczurek, et al. Hollow carbon spheres in microwaves: Bio inspired absorbing coating. *Applied Physics Letters*, 108(1):013701, 2016.

[15] H. Angus Macleod and H. Angus Macleod. *Thin-film optical filters*. CRC press, 2010.

[16] Henry W Ott and Henry W Ott. *Noise reduction techniques in electronic systems*, volume 442. Wiley New York, 1988.

[17] Edgar Hund. *Microwave Communications: components and circuits*. Glencoe/McGraw-Hill School Publishing Company, 1989.

[18] Evgeni Ivanov, Rumiana Kotsilkova, Hesheng Xia, Yinghong Chen, Ricardo K. Donato, Katarzyna Donato, Anna Paula Godoy, Rosa Di Maio, Clara Silvestre, and Sossio Cimmino. Pla/graphene/mwcnt composites with improved electrical and thermal properties suitable for fdm 3d printing applications. *Applied Sciences*, 9(6):1209, 2019.

[19] Rumiana Kotsilkova, Ivanka Petrova-Doycheva, Dzhihan Menseidov, Evgeni Ivanov, Alesya Paddubskaya, and Polina Kuzhir. Exploring thermal annealing and graphene-carbon nanotube additives to enhance crystallinity, thermal, electrical and tensile properties of aged poly (lactic) acid-based filament for 3d printing. *Composites Science and Technology*, 181:107712, 2019.

[20] Standard test method for measuring relative complex permittivity and relative magnetic permeability of solid materials at microwave frequencies, astm d5568-08, 2009.

[21] Boon-Kuan Chung. Dielectric constant measurement for thin material at microwave frequencies. *Progress In Electromagnetics Research*, 75:239–252, 2007.

[22] D. Bychanok, P. Kuzhir, S. Maksimenko, S. Bellucci, and Christian Brosseau. Characterizing epoxy composites filled with carbonaceous nanoparticles from dc to microwave. *Journal of Applied Physics*, 113(12):124103, 2013.

[23] Dzmitry Bychanok, Polya Angelova, Alesia Paddubskaya, Darya Meisak, Lizaveta Shashkova, Marina Demidenko, Artyom Plyushch, Evgeni Ivanov, Rumen Krastev, and Rumiana Kotsilkova. Terahertz absorption in graphite nanoplatelets/polylactic acid composites. *Journal of Physics D: Applied Physics*, 51(14):145307, 2018.

[24] Chloé Méjean, Laura Pometcu, Ratiba Benzerga, Ala Sharaiha, Claire Le Paven-Thivet, Mathieu Badard, and Philippe Pouliguen. Electromagnetic absorber composite made of carbon fibers loaded epoxy foam for anechoic chamber application. *Materials Science and Engineering: B*, 220:59–65, 2017.

[25] H Nornikman, F Malek, PJ Soh, AAH Azremi, and A Ismahayati. Reflection loss performance of triangular microwave absorber. In *International Symposium on Antennas and Propagation (ISAP 2010)*, 2010.

[26] Ilona Piekarz, Jakub Sorocki, Izabela Slomian, Krzysztof Wincza, and Slawomir Gruszczynski. Experimental verification of 3d printed low-conductivity graphene-enhanced pla absorbers for back lobe suppression in aperture-coupled antennas. In *2018 IEEE-APS Topical Conference on Antennas and Propagation in Wireless Communications (APWC)*, pages 780–782. IEEE, 2018.

[27] S. Adachi, M. Hattori, F. Kanno, K. Kiuchi, T. Okada, and O. Tajima. Production method of millimeter-wave absorber with 3d-printed mold. *Review of Scientific Instruments*, 91(1):016103, 2020.

[28] Y Zhu, L Liu, Y Zhang, QC Luo, YH Qi, F Yu, and

FH Li. Development of millimeter-wave em absorber with homogenization theory. *SN Applied Sciences*, 1(5):398, 2019.